Article

Investigation into Dynamic Pressure Pulsation Characteristics in a Centrifugal Pump with Staggered Impeller

Dan Ni [1,2,*], **Jinbo Chen** [1], **Feifan Wang** [1,2], **Yanjuan Zheng** [3], **Yang Zhang** [3] **and Bo Gao** [1]

[1] School of Energy and Power Engineering, Jiangsu University, Zhenjiang 212013, China
[2] Shanghai Kaiquan Pump (Group) Co., Ltd., Shanghai 201800, China
[3] Shanghai Marine Equipment Research Institute (SMERI), Shanghai 200031, China
[*] Correspondence: nidan@ujs.edu.cn

Abstract: For the centrifugal pump, the rotor–stator interaction (RSI) induces high-energy pressure pulsation, which directly affects the stability of systems and equipment. Therefore, this work proposes a new staggered impeller structure to suppress high-energy pressure pulsation in centrifugal pumps. The original impeller blade is divided into two layers and is staggered at 10°, 20° and 30° to form a staggered impeller. The dynamic pressure pulsation characteristics of both the original impeller and the staggered impeller are predicted using large eddy simulation (LES). The results indicate that the uniform staggered arrangement of blades can significantly reduce the pressure pulsation energy in the pump by 54.69% under the design conditions, while also achieving the best performance. Even under off-design conditions, the pressure pulsation energy can still be effectively suppressed by the staggered blades. The study of the time–frequency domain of the monitoring points near the tongue found that the phase difference in the pressure fluctuation caused by the RSI between the staggered impeller and the tongue prevents the superposition of pressure pulsation energy and efficiently suppresses it in the pump. The results can provide a reference for optimizing low-vibration-noise pump impellers in engineering applications.

Keywords: centrifugal pump; staggered impeller; numerical simulation; pressure pulsation; phase difference

1. Introduction

Centrifugal pumps are definitely of interest in a wide range of applications in medicine [1], chemistry and biology [2,3], as well as micro-fluidics and nano-fluidics [4–6]. For efficient and stable operation, the low vibration and noise characteristics, as well as the ultra-low pressure pulsation characteristics of centrifugal pumps, are also gaining attention [7,8]. However, the strong rotor–stator interaction (RSI) in the centrifugal pump is the primary source of high-energy pressure pulsation, which can cause damage to the impeller and other hydraulic components [9]. To improve the stability and safety of the system, it is crucial to suppress the pressure pulsation characteristics in centrifugal pumps.

In recent years, the study of pulsation in centrifugal pumps and fans has been a fairly common research direction. The method of numerical simulation is widely used in research. Ding et al. [10] analyzed the effect of the blade trailing edge filing on the performance and unsteady pressure pulsations of a low-specific-speed centrifugal pump using the *SST k-ω* turbulence model. In the research of Jiang et al. [11] and Zhao et al. [12], the results obtained by the *SST k-ω* model deviated somewhat from the experiment. In recent years, more advanced DES (detached eddy simulation) and LES (large eddy simulation) methods have been widely used with an improvement in computer performance. Gangipamula et al. [13] studied the fluid dynamic characteristics of a narrow channel centrifugal pump via DES. Based on the same turbulence model, Wang et al. [14] successfully captured the axial vortex in a centrifugal pump as a turbine with an S-Blade impeller. From the research by Cai et al. [15], the DES method could accurately predict pressure pulsations

in centrifugal fans and their downstream pipe, which agreed well with the experimental results. Considering that the DES method is more resource-intensive, Posa and Zhang et al. [16,17] predicted the complex flow structure in the pump based on the LES calculation method. The study found that pressure pulsation amplitude increased under the small flow rates, the discrete characteristic frequency components were rich in the low-frequency band and the amplitude of f_{bpf} increased significantly. The pressure fluctuation energy induced by the RSI is dominant in unsteady hydraulic excitation.

Based on RSI theory, Gülich and Rodriguez [18,19] deduced the formula of the excitation frequency generated by the RSI of the impeller–diffuser under the given combination of the different blade numbers. Meanwhile, the formula for judging the mode shape of the impeller under the RSI was given for the designer's reference to select the appropriate number of blades. Spence [20] studied the effects of four geometric parameters on the pressure pulsation of centrifugal pumps. Increasing the gap between the impeller and the volute was found to effectively and reasonably reduce the amplitude of pressure pulsation [21]. However, a larger gap would reduce head and efficiency [22].

In the study of unique impeller structures, adding splitter blades could effectively improve performance and suppress the pressure pulsation in the pump [23,24]. Zhang and Gu et al. [25–27] studied the effect of splitter blades on the flow characteristics in the pump via experiments and numerical simulation and found that splitter blades can effectively optimize the jet wake structure, improve the internal flow structure of the impeller channel and reduce the pressure fluctuation in the pump. In double-suction centrifugal pumps, a back-to-back impeller structure with staggered blades is widely used to reduce the radial force distribution and pump vibration [28,29]. Zeng and Fu et al. [30,31] found that the staggered impeller had little effect on the performance of a double-suction pump, and the pressure pulsation level in the volute was significantly reduced when the blade was evenly staggered.

In the present paper, referring to the design idea of the double-suction pump, a staggered impeller structure is proposed in the single-suction low-specific-speed centrifugal pump. The dynamic pressure pulsation characteristics are investigated using the LES method. Emphasis is laid on the pressure pulsation energy caused by different impeller structures under various operating conditions. In addition, the time–frequency domain of pressure pulsation at each measurement point near the tongue was analyzed. The suppression mechanism of the low-frequency signal induced by dynamic and static interference via the staggered impeller was elucidated. The research results can provide a reference for optimizing low-vibration-noise pump impellers.

2. Case Study and Numerical Investigation

2.1. Model Pump Scheme

To reduce the influence of complex parameters on the pressure pulsation characteristics in the model pump and reduce the difficulty of design and processing, a single-stage, single-suction centrifugal pump with low specific speed (n_s = 69) was the object of the current study. The main parameters are shown in Table 1.

Table 1. Main design paraments of the model pump.

Main Geometric Data	Value
Nominal flow rate Q_N	0.0153 m^3/s
Nominal head H_N	20 m
Nominal rotational speed n	1450 rpm
Impeller outlet width b_2	17 mm
Blade number Z	6
Exit circumferential velocity u_2	19.74 m/s
Nominal head coefficient $\Psi_N = gH_N/u_2{}^2$	0.605
Specific speed n_s	69
Pressure coefficient C_p	$(P_i - P_{av})/0.5\rho u_2{}^2$

The original blades were divided into the front and the posterior layer blade, which were connected by a diaphragm. The original and staggered impellers are shown in Figure 1. The thickness of the diaphragm was 3 mm. The original scheme is defined as Or. After the blades were staggered by 10°, 20° and 30°, three staggered impeller schemes, St10, St20, and St30, were formed. The different staggered impeller schemes are shown in Figure 2. The total width of the front and posterior impeller outlet was still 17 mm.
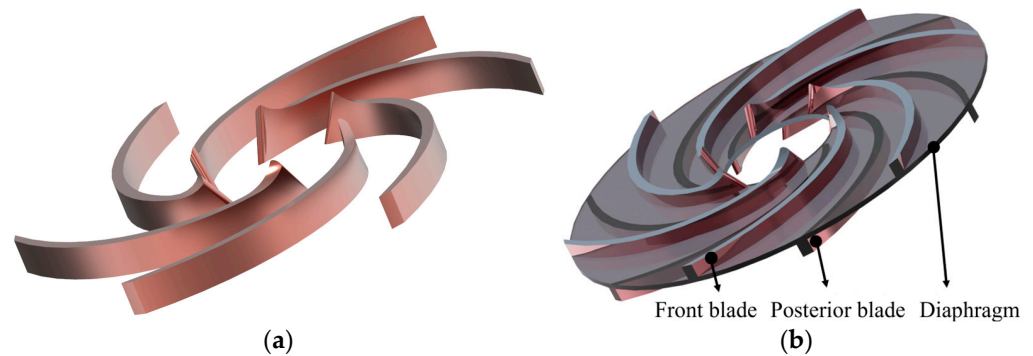

Figure 1. The impeller in the pump. (**a**) Original impeller; (**b**) staggered impeller.
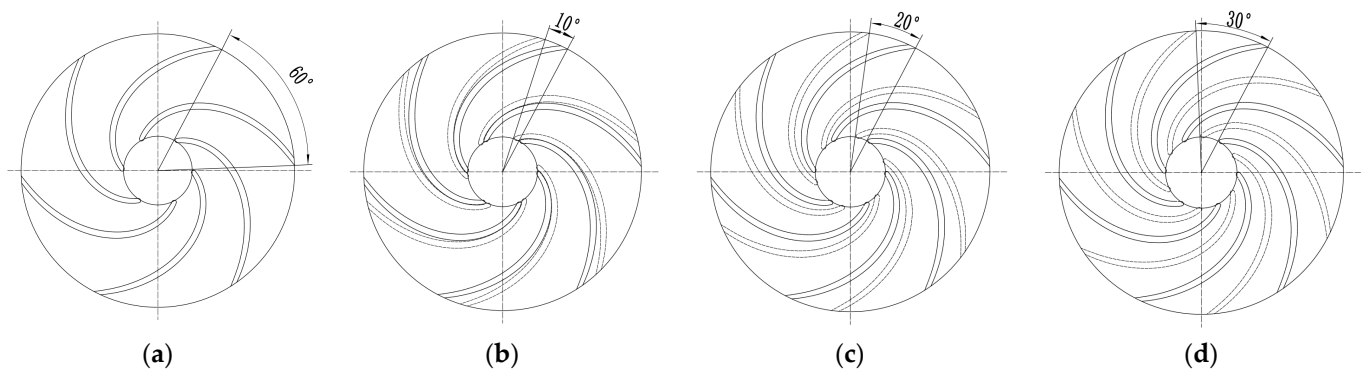
Figure 2. Different impeller models. (**a**) Original impeller (Or); (**b**) staggered 10° (St10); (**c**) staggered 20° (St20); (**d**) staggered 30° (St30).

2.2. Mesh Generation

The calculation domain of the model pump includes four parts: the inlet section, the impeller, the volute and the outlet section. To improve the calculation accuracy, the inlet and outlet sections are properly extended to ensure that they do not affect the flow structure within the impeller and volute. The structured grid can be easily fitted to the boundary in a fast and high-quality manner. The hexahedral structured grid can well control the orthogonal boundary layer and streamline distribution. It exhibits good truncation error and convergence throughout the numerical calculation process. Moreover, it is suitable for calculating fluid and surface stress concentration in the centrifugal pumps. Therefore, ANSYS-ICEM was used in this paper to generate the structured mesh grids of the computational domain, as shown in Figure 3a. Furthermore, the boundary layer encryption was applied to the areas where the pressure gradient in the pump was high, and it was easy for flow separation to occur, especially on the blade wall. The wall encryption of the impeller flow channel is shown in Figure 3b. A small Y plus value was required to obtain a better flow structure of the model pump, especially for the impeller. Figure 3c gives the Y plus value on the blade surface for the current study. During the simulation, the Y plus insensitive treatment was used by the *SST k-ω* turbulent model to treat the flow field near the solid wall, which could automatically dispose the mesh near the wall. It is noted that the average Y plus value for the impeller was about 5 and was lower on the pressure surface. We believed that using refined mesh could meet the calculation requirements of LES and obtain accurate numerical simulation results.

(**a**)

(**b**)

(**c**)
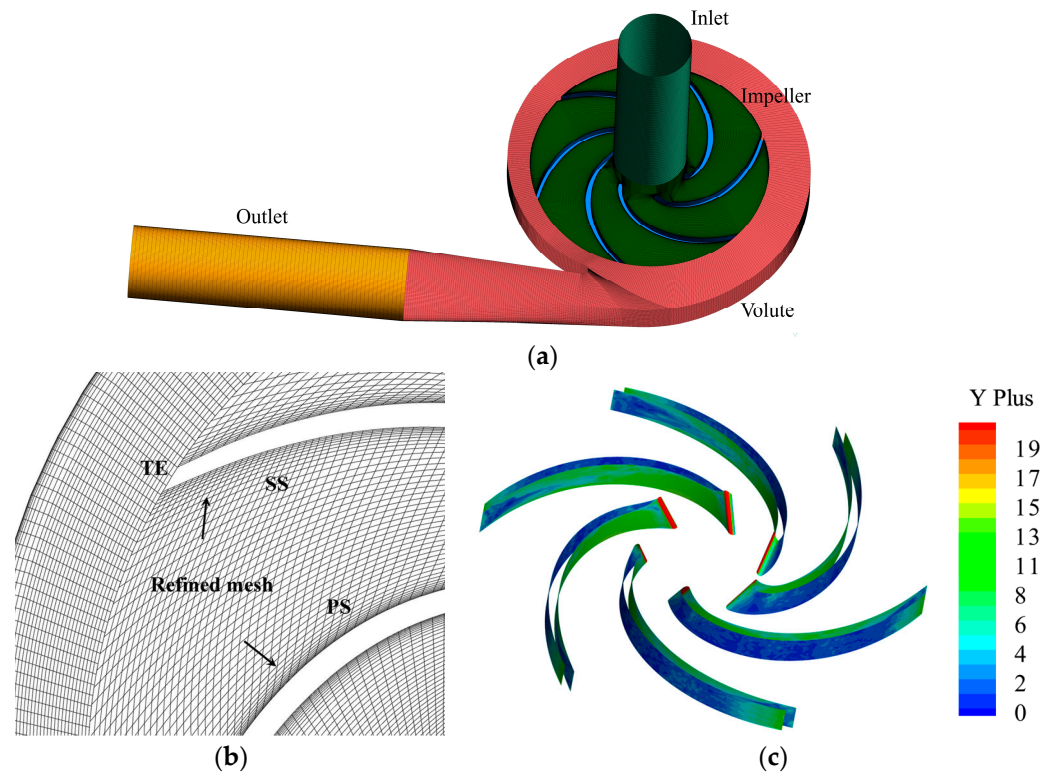
Figure 3. Structured grids for fluid computing domain. (**a**) The structured grid partition of the entire computational domain; (**b**) the wall encryption of the impeller; (**c**) Y plus values in the impeller.

Seven different grid number schemes were designed to check the mesh's sensitivity. The performance of different grid number schemes was predicted under the rated flow rate, and the change in hydraulic efficiency was monitored, as seen in Figure 4. The efficiency of the model pump gradually decreased as the number of grids increased. When the number of grids exceeded 7.94×10^6, the efficiency tended to be flat. When the accuracy and computational resource usage were considered, the total grid number was 7.94×10^6, and the impeller grid number was 4.0×10^6.
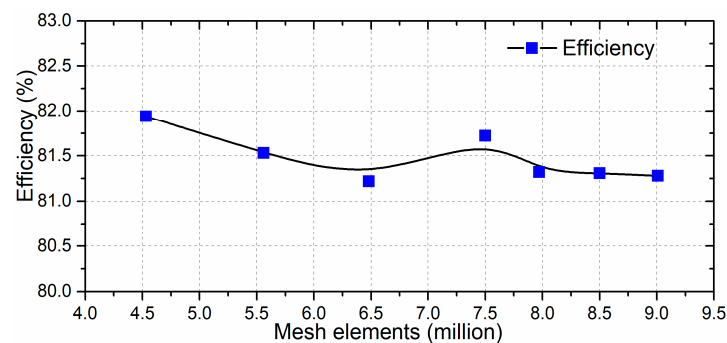
Figure 4. Mesh sensitivity check.

2.3. Solution Parameters

In this study, the SIMPLEC algorithm was used to couple pressure and velocity. The steady-state results calculated using the *SST k-ω* model were used as the initial conditions for unsteady-state calculations. The *SST k-ω* model combines the advantages of the traditional *k-ε* and *k-ω* models, which can better deal with the flow separation near the wall. Considering that the large eddy simulation (LES) model has sufficient ability to deal with complex flows, it was applied for the prediction of unsteady pressure pulsation characteristics [32,33]. For incompressible fluids, a filter and a continuity equation

were added to the N-S equation to obtain the momentum equation, which is defined in Equation (1):

$$\frac{\partial \overline{u_i}}{\partial t} + \frac{\partial}{\partial x_j}(\overline{u_i u_j}) = -\frac{1}{\rho}\frac{\partial \overline{p}}{\partial x_i} + \frac{\partial}{\partial x_j}\left[\nu(\frac{\partial \overline{u_i}}{\partial x_j} + \frac{\partial \overline{u_j}}{\partial x_i})\right] + \frac{\partial \overline{\tau_{ij}}}{\partial x_j} + S_i \tag{1}$$

The Smagorinsky–Lilly subgrid scale (SGS) fixed-coefficient model [7] was applied to close the equations, which is defined in Equation (2).

$$\overline{\tau_{ij}} - \frac{1}{3}\delta_{ij}\overline{\tau_{kk}} = -2\nu_T \overline{S_{ij}} \tag{2}$$

where $\overline{S_{ij}}$ is the strain rate tensor and v_T is the SGS stress viscosity.

$$v_T = (C_s\Delta)^2|\overline{S}| \tag{3}$$

$$|\overline{S}| = \sqrt{2\overline{S_{ij}}\overline{S_{ij}}} \tag{4}$$

where Δ is the filter scale and $C_S = 0.1$ is a dimensionless parameter called the Smagorinsky coefficient.

The inlet boundary condition is a uniform velocity inlet, which is given according to the operating conditions and the inlet suction diameter. The specific turbulence characteristics are given, where the turbulence intensity is 5%. The outlet boundary condition is the pressure outlet. In numerical calculations, all physical walls are non-slip walls. Second-order implicit time discretization was used, and the calculated residual was set to 1×10^{-6}.

2.4. Monitoring Points

To explore the influence of the staggered impeller on the pressure pulsation characteristics in the pump, 20 uniformly distributed pressure pulsation monitoring points were set up in the volute, near the front cover of the impeller, as shown in Figure 5. The pressure fluctuation signals from the last 15 rotation cycles of the numerical calculation results were processed and analyzed. The Hanning window function [34] reduces the energy leakage caused by signal truncation. It is a bell-shaped curve that is symmetric around the middle of the interval. The Hanning window touches zero at both ends, removing any discontinuity, while the traditional window functions, such as the rectangular window, stop just shy of zero, meaning that the signal will still have a slight discontinuity. It is defined as follows:

$$w_{\text{H}}(n) = \begin{cases} 0.5\left[1 - \cos(2\pi\frac{n}{N})\right] & 0 \le n = N-1 \\ 0 & \text{otherwise} \end{cases} \tag{5}$$
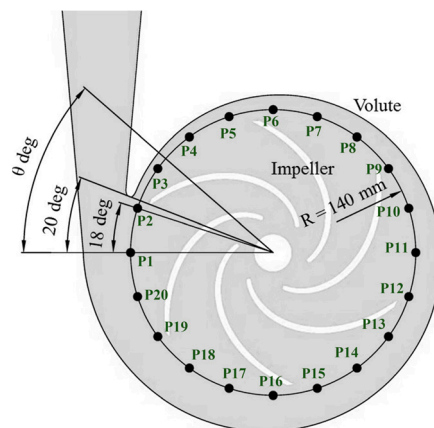

Figure 5. Pressure pulsation monitoring points.

2.5. Experimental Platform

The original impeller model pump was tested on the closed test platform to verify the reliability of the numerical method [35], as shown in Figure 6. The high-precision pressure test equipment was used to measure the pressure information in the model pump. The SCM05 model of Belgium LMS company was used for data acquisition, and the pressure sensor was the PCB113B27X model of the American PCB company. The water temperature was maintained at about 25° throughout the test. The inverter was used to ensure that the speed of the model pump at different flow rates was about n = 1450 rpm. The arrangement of the pressure fluctuation test points is shown in Figure 7.
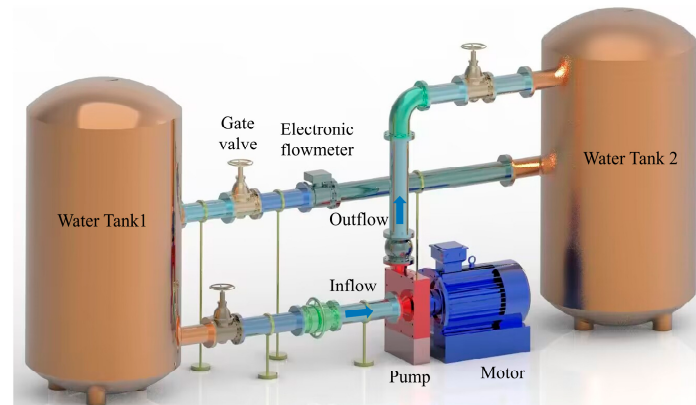

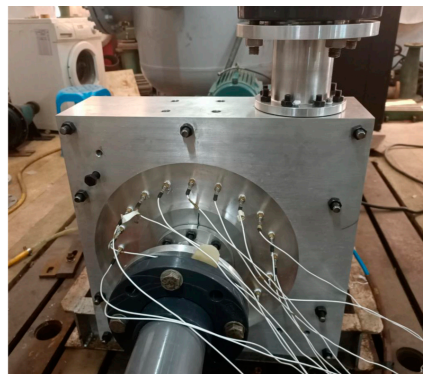**Figure 6.** Model pump closed test platform.

Figure 7. Experimental picture of the original model pump.

3. Results

3.1. Validation of the Numerical Method

The accuracy of the numerical method was verified based on the experimental results of the original impeller model pump. The comparison results of the head coefficients of different calculation methods are shown in Figure 8. The head coefficient curve predicted by the LES method is more consistent with the experimental value under large flow conditions. Under rated conditions, the prediction error is only about 0.5%. The predicted head of the RANS method is slightly lower than the experimental value, and the error is 3% under the design condition.

In order to verify the reliability of the LES calculation method, Figure 9 compares the LES calculation and the experimental results of the 20 pressure pulsation monitoring points in the circumferential direction of the volute under the design conditions. It can be found that the predicted dominant frequency amplitude of each monitoring point is in good agreement with the experimental results, and there is almost no error at the measuring points, such as P1 and P5. In order to further verify its reliability, Table 2 extracts the average error of amplitude at the blade frequency (f_{bpf}) and 2 times blade frequency ($2f_{bpf}$)

of 20 measuring points in the experiment and simulation. It can be found that the average error of amplitude at f_{bpf} predicted by the LES numerical calculation method is 13.85%, while that of amplitude at $2f_{bpf}$ is only 2.24%. Therefore, the LES method can accurately predict the pressure fluctuation characteristics of the low-specific-speed centrifugal pump.
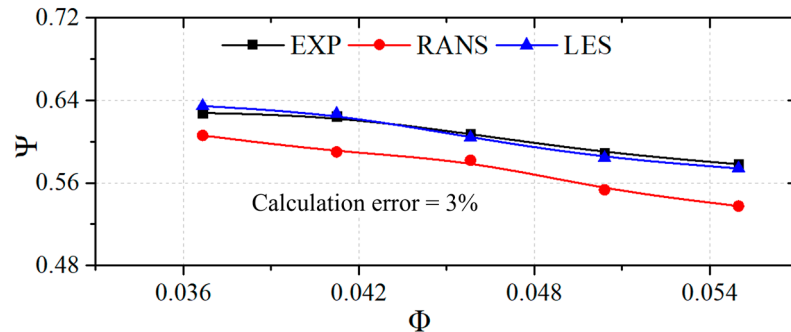

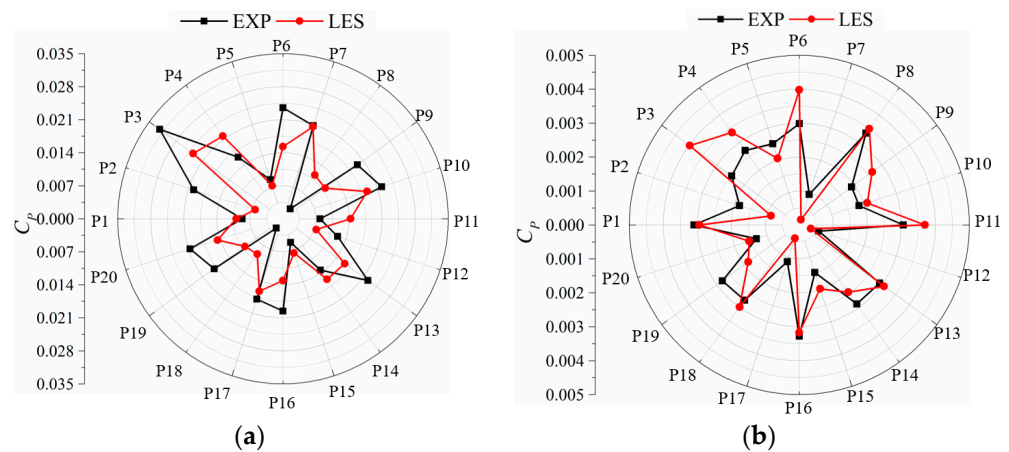**Figure 8.** Head coefficient comparison.

Figure 9. Comparison of experimental and simulated main frequency amplitude. (**a**) Amplitude at f_{bpf}; (**b**) amplitude at $2f_{bpf}$.

Table 2. Simulated prediction of main frequency amplitude mean error.

Parameter	EXP	LES	Δ
f_{bpf}	0.0153466	0.0133380	13.08%
$2f_{bpf}$	0.0023320	0.0023854	2.24%

3.2. Unsteady Pressure Pulsations

For the convenience of analysis, the pressure signal was non-dimensionalized and the pressure fluctuation coefficient was defined as follows:

$$C_p = (P - P_{av})/0.5\rho u_2^2 \tag{6}$$

In the equation, P is the pressure of the monitoring point; P_{av} is the average pressure of the monitoring points; ρ is the water density and u_2 is a constant value of 19.74 m/s.

### 3.2.1. Overall Pressure Pulsation Energy Analysis

The numerical calculation of pressure pulsation in different staggered impeller models was carried out to explore the influence of different staggered impeller structures on the pressure pulsation energy in the pump. Q/Q_d = 0.8, 1.0 and 1.2 were selected for comparative analysis. The root mean square error (*RMSE*) was used to characterize the pressure pulsation energy in the pump, as shown in Equation (7). The amplitude information of

20 pressure pulsation monitoring points in the 10–1000 Hz frequency band was processed using *RMSE*.

$$RMSE = \sqrt{\sum_{i=1}^{n} (C_{Pi} - \overline{C}_P)^2 / N} \tag{7}$$

In the equation, C_{Pi} is the pressure coefficient value of the measuring point, C_P is the average value of the pressure coefficient and N is the number of samples of the measured pressure coefficient.

Figure 10 shows the pressure fluctuation energy distribution of different impeller schemes under different working conditions. It can be found that the highest point of the pressure pulsation energy of the four impeller schemes under different working conditions appears near the P3 point downstream of the tongue. As a result, the vicinity of the tongue is the site of the most rotor–stator interaction (RSI) in the pump, causing high-intensity pressure pulsation to peak downstream in the tongue.
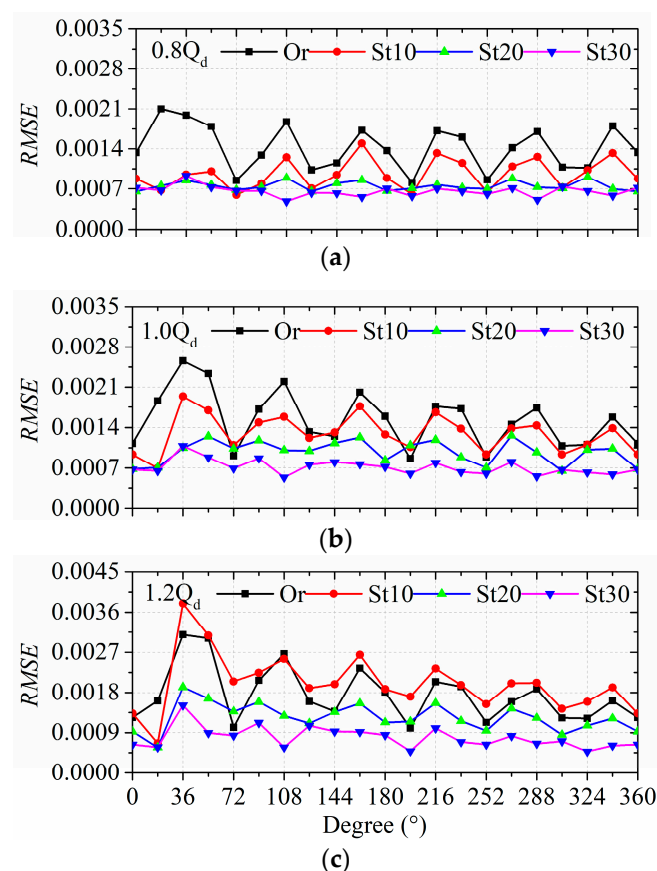
Figure 10. Pressure pulsation energy distribution of different working conditions. (**a**) *RMSE* distribution at $0.8Q_d$; (**b**) *RMSE* distribution at $1.0Q_d$; (**c**) *RMSE* distribution at $1.2Q_d$;

Additionally, it was discovered that the staggered arrangement of blades significantly reduces the pressure pulsation energy in the pump within the 10–1000 Hz range, and the suppression impact increases with the staggered angle. The optimum effect results from evenly spaced blades. Compared with the design condition, under the condition of $0.8Q_d$, the peak value of the pressure fluctuation energy of the Or scheme is transferred to the P2 point, indicating that the RSI between the impeller and the tongue is weak under the low flow condition, and the pressure fluctuation energy decreases with increasing distance from the tongue. Under the condition of flow $1.2Q_d$, the pressure pulsation energy level increases when the blade is staggered by 10°, and this is gradually suppressed as the staggered angle increases.

From the overall comparison, it can be found that the staggered arrangement of the blades has the most significant suppression effect on the pressure pulsation energy at points P1–P3 near the tongue.

The suppression effect of the staggered impeller structure on the pressure pulsation energy in the pump was quantified by calculating the *RMSE* mean change, and the calculation method is shown in Equation (8). Table 3 shows the reduction in the *RMSE* mean value of different impeller schemes under three working conditions. From the table, it can be seen that under different working conditions, the St30 scheme, that is, the uniform staggered blade, has the best suppression effect on the pressure pulsation energy in the pump, and the suppression amplitude is above 50%.

$$\Delta \overline{RMSE} = (\overline{RMSE}_{St} - \overline{RMSE}_{Or}) / \overline{RMSE}_{Or} \tag{8}$$

Table 3. RMSE value reduction in different impeller schemes under different working conditions.

Case	St10	St20	St30
$0.8Q_d$	−15.58%	−37.70%	−53.39%
$1.0Q_d$	−30.36%	−47.10%	−54.69%
$1.2Q_d$	+14.48%	−29.33%	−54.95%

3.2.2. Pressure Pulsation Energy Analysis near the Tongue

The pressure pulsation energy in the pump is mainly determined by the energy of the main frequency amplitude, and the pressure pulsation energy near the tongue is dominant. The above analysis shows that the staggered impeller has the most apparent effect on the pressure pulsation energy near the tongue. In order to study the suppression mechanism of the staggered impeller structure on pressure pulsation energy, the pressure pulsation characteristics of three monitoring points P1, P2, and P3 of the St30 scheme under design conditions were studied in depth, and pressure pulsation monitoring points were set at the center outlet of the front and the posterior impeller. The new measuring points were on the central section of the two-layer impeller outlet. One was the same radius as the above analysis measuring point, and the other was close to the edge of the impeller outlet. The measuring points of P1-(i), P2-(i) and P3-(i) were set as shown in Figure 11. The pressure pulsation data of each monitoring point were extracted to obtain the time–frequency characteristics, which were then analyzed based on the short-time Fourier transform.
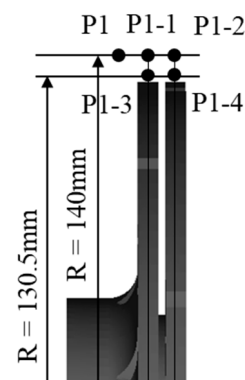
Figure 11. Schematic diagram of new measuring points on the outside of the impeller.

Figure 12 shows the pressure pulsation time–frequency domain diagram for the Or scheme at monitoring points P1, P2 and P3. It can be seen from Figure 12a that the main characteristic frequency signals at point P1 are mainly f_{bpf} and $2 f_{bpf}$, and are continuous during the sampling time. Point P2 is facing the tongue, and the RSI is most intense near the point. Therefore, it is clear from Figure 12b that the characteristic frequency signals are mainly messy low-frequency signals in the sampling time, which are more chaotic in the

time domain. Additionally, the frequency amplitude is generally larger in the 0–145 Hz bandwidth. As can be seen from Figure 12c, the main characteristic frequency signal at this point is mainly f_{bpf}, which has a large bandwidth and is extremely continuous during the sampling time. The pressure pulsation energy is also the strongest at this point, which is consistent with the results analyzed in Figure 10.
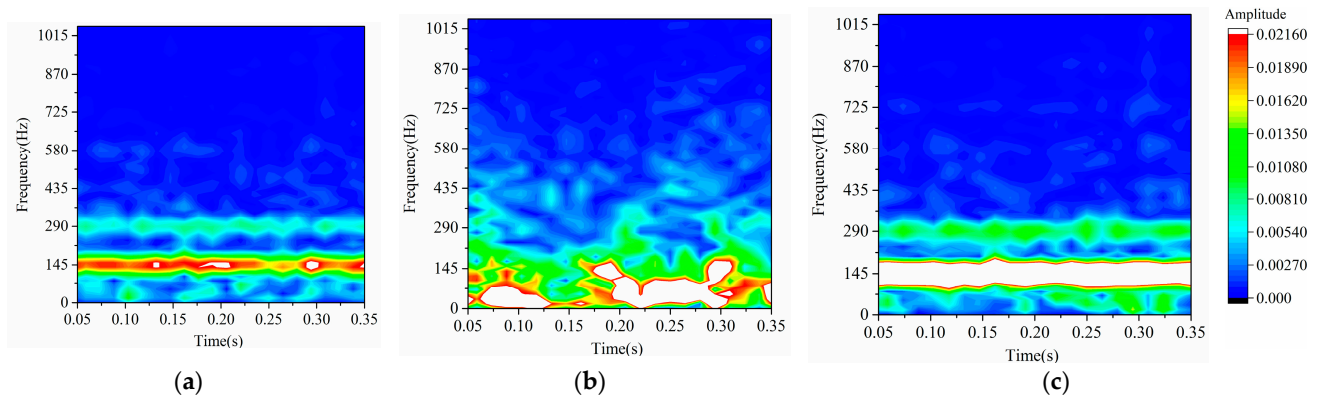
Figure 12. Time–frequency domain analysis chart of original impeller pressure pulsation. (**a**) P1. (**b**) P2. (**c**) P3.

Figure 13 shows the time–frequency domain characteristics of the monitoring points at the staggered impeller outlet (P1-1, P1-2, P2-1, P2-2, P3-1 and P3-2), which correspond to the points P1, P2 and P3 at the central exit of the original impeller. As can be seen from P1-1 and P1-2, the main frequency of P1 changed from f_{bpf} to 2 f_{bpf} during the sampling time after the blades were evenly staggered. Compared with the Or scheme, it is easy to find that the occurrence time of high-energy signals near f_{bpf} in the St30 scheme is staggered during the sampling time, which can avoid intensity superposition. P2-1 and P2-2 show that the staggered arrangement of blades significantly suppresses the disorderly low-frequency signals, and the high-amplitude signals in the low-frequency band almost disappear compared to the Or scheme. In P3-1 and P3-2, the f_{bpf} signal also produces a high amplitude at different moments, while the high-amplitude signals in the Or scheme are very continuous in the time domain.

According to this analysis, the high-speed outflow of the front and posterior impellers interferes with the tongue in turn when the blades are staggered uniformly to sweep it. The induced high-amplitude blade frequency signal is then staggered during the sampling time, avoiding an intensity overlap in the time domain. Therefore, the impeller structure with uniformly staggered blades can make the pressure pulsations induced by the RSI exist with a certain phase difference, thus effectively suppressing the low-frequency pressure pulsation energy.

In order to clarify the phase difference in the pressure pulsation in the pump caused by the staggered impeller, the radius of the above monitoring points was changed to be close to the impeller outlet to reduce the interference of unsteady hydraulic excitation on the pressure pulsation signal. The monitoring points are shown in Figure 11. The pressure pulsation data of the monitoring points P1-3, P1-4, P2-3, P2-4 and P3-4 corresponding to the three points P1, P2 and P3 on the upper and lower reaches of the tongue were extracted.

Figure 14 shows the time domain diagram of the pressure pulsation at the outlet of the staggered impeller at three measuring points during a rotation period. In the above analysis, the two impellers of the front and posterior layers interfere with the tongue separately, and there is a lead and lag in timing. It can be seen in the time domain diagram that due to the existence of blade thickness, the pressure pulsation drops sharply at the valley value when the blade sweeps through the measuring point position, and there is a noticeable 30 ° phase difference in the valley value. At the same time, the phase difference at the peak of the pressure pulsation can be found at different measuring points. It is the existence of the phase difference that effectively avoids the superposition of high-energy pressure

pulsation amplitude and achieves the purpose of suppressing the pressure pulsation energy in the pump.
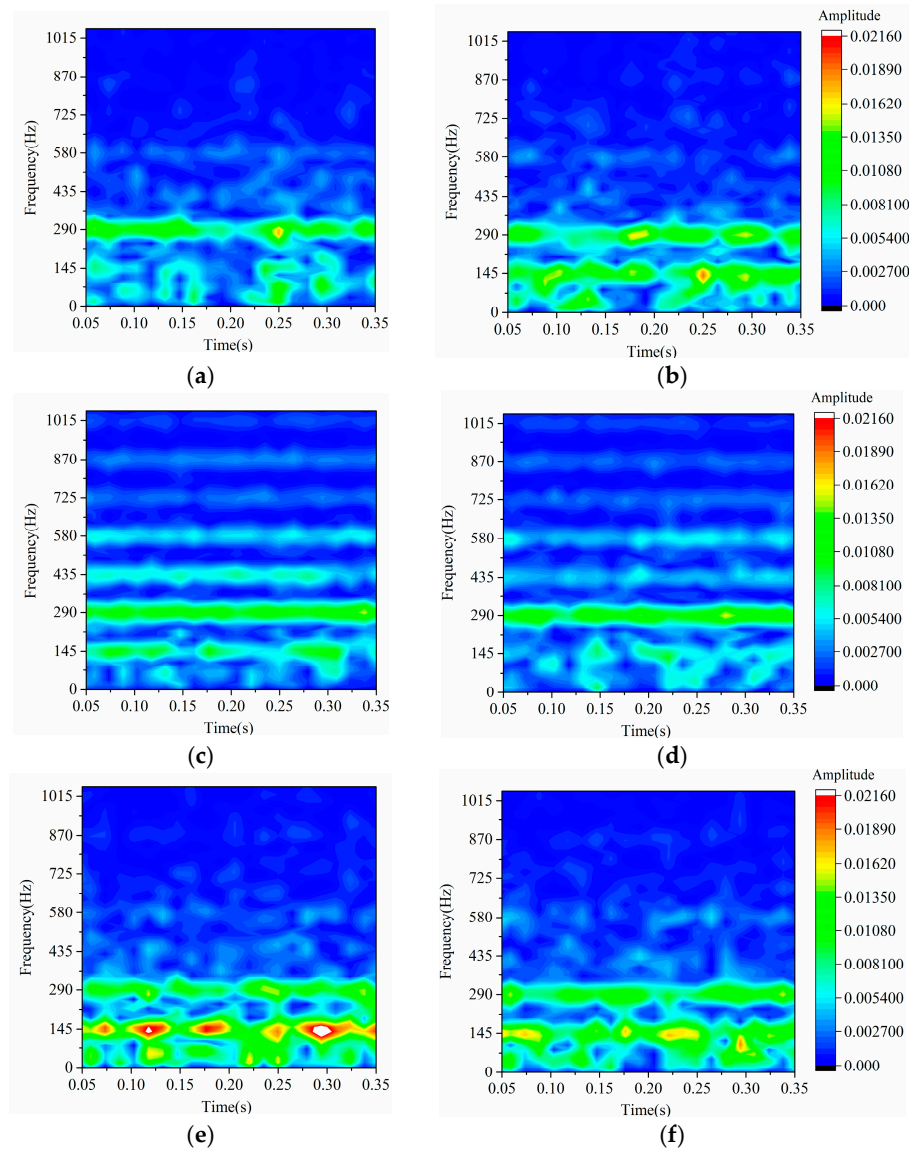
Figure 13. Time–frequency domain analysis of pressure pulsation at the outlet monitoring point of the staggered impeller. (**a**) P1-1. (**b**) P1-2. (**c**) P2-1. (**d**) P2-2. (**e**) P3-1. (**f**) P3-2.
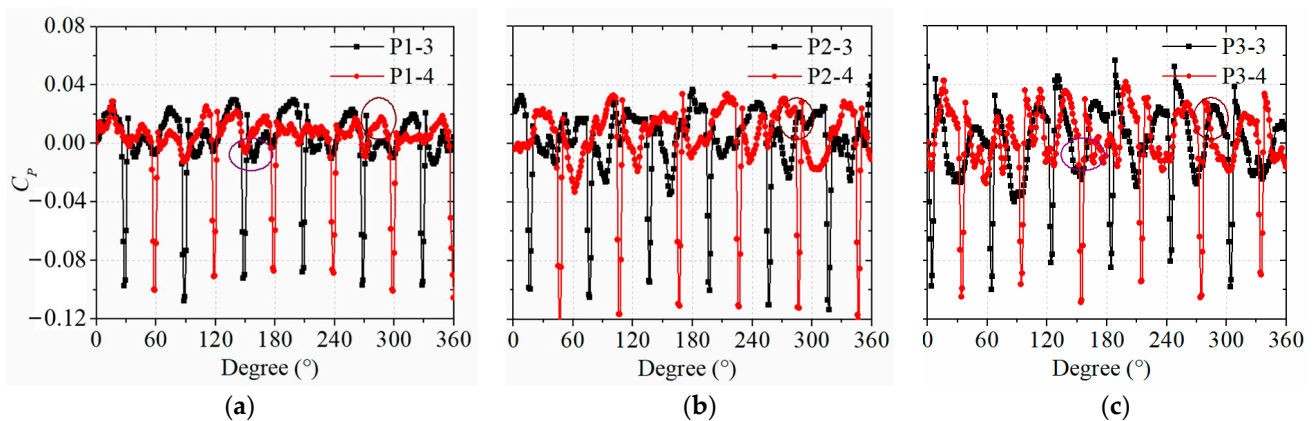
Figure 14. Time domain diagram of pressure fluctuation at the outlet of the staggered impeller. (**a**) P1-3 and P1-4. (**b**) P2-3 and P2-4. (**c**) P3-3 and P3-4.

4. Discussion

The centrifugal pump is of great interest in all industrial fields. The dynamic pressure pulsation will be essential to the stable running of the pump and also the related pumping system. In the present paper, a model pump with the original impeller and three staggered impellers were investigated. The main focus was placed on the pressure pulsation energy induced by the RSI effect.

In recent years, numerical simulation methods have been widely used to capture pressure pulsation characteristics. Despite the shortcomings of the RANS model, it has always been the most commonly used and the most popular. However, in the experimental study, it was verified that the RANS model is somewhat less accurate. Therefore, this paper used the more advanced LES method to investigate the model pump, which is closer to the experimental results.

In the published research, scholars have proposed various methods to suppress the pressure pulsation in the pump. However, there are still problems, such as interference frequency energy and low-frequency energy suppression [23], as the researchers concluded that RSI is the main cause of pressure pulsation in the pump. Even though the RSI has been investigated by many scholars, the influence of the staggered impeller structure on the pressure fluctuation energy in the centrifugal pump has not been comprehensively revealed.

Three staggered impeller structures with different angles were designed in the present work. The dynamic pressure pulsation characteristics were obtained and compared using the LES method. Via the overall evaluation of the pressure pulsation at 20 measurement points of different impeller model pumps, it was found that the pressure pulsation energy of the model pump decreases by more than 50% when the blades are evenly staggered under different working conditions. According to the analysis of the time–frequency domain of pressure pulsation near the tongue, the staggered impeller structure makes the unsteady pressure pulsation generated by the interference of the impeller discharge fluid and the tongue produce a phase difference in the time domain, avoiding the superposition of high-energy pressure pulsation energy, thereby reducing the overall pressure pulsation intensity of the pump.

In a further study, we expect to reveal the effect of a staggered impeller structure on flow-induced noise in centrifugal pumps using high-precision hydrophones. This would be essential for the optimization design of a low-vibration-noise pump.

5. Conclusions

In the present paper, a low-specific-speed centrifugal pump was taken as the research object. Pumps with the original impeller model and three staggered impeller models were created. The dynamic pressure pulsation characteristics were investigated, especially near the tongue. The experiment first validated the applied LES method.

Emphasis was laid on the pressure pulsation energy caused by different impeller structures under various operating conditions. In addition, the time–frequency domain of pressure pulsation at each measurement point near the tongue was analyzed. Finally, some conclusions were obtained, as follows.

From comparison with the experimental results, it was validated that the applied LES method with the refined structured mesh can accurately predict the pressure fluctuation characteristics of the model pump. The predicted dominant frequency amplitude of each measurement point was obtained at various flow rates.

From the comparative analysis of the overall pressure pulsation energy caused by different impeller structures, it was concluded that the uniform staggered blade has the best suppression effect on the pressure pulsation energy in the model pump, especially near the tongue area. The overall suppression amplitude was above 50%.

According to the analysis of the time–frequency domain of pressure pulsation near the tongue, the high-amplitude interference frequency signals induced by the RSI between the staggered impellers and the tongue were staggered during the sampling time, and the

peaks of the pulsating waves were staggered in the time domain to form a phase difference. Thus, the low-frequency pressure pulsation energy was effectively suppressed.

The staggered impeller in a low-specific-speed single-suction centrifugal pump can greatly suppress the pressure pulsation in the pump, reducing the vibration and noise. It can provide a reference for optimizing low-vibration-noise pump impellers in engineering applications.

Data Availability Statement: No new data were created or analyzed in this study. Data sharing is not applicable to this article.

Conflicts of Interest: The authors declare no conflict of interest.

Abbreviations

Acronyms

ECT	Et cetera
RMSE	Root mean square error

Symbols

$\overline{A_P}$	The average value of f_{bpf} amplitude
f_{bpf}	Blade passing frequency
Q_N	Nominal flow rate
H_N	Nominal head
n	Nominal rotational speed
b_2	Impeller outlet width
Z	Blade number
u_2	Circumferential velocity of the impeller outlet
Ψ_N	Nominal head coefficient
n_s	Specific speed
D_1	Impeller inlet diameter
D_2	Impeller outlet diameter
δ	Thickness of partition plate
f_r	Shaft frequency signal
C_p	Pressure coefficient C_p
E_Q	Flow measurement uncertainty
η	Efficiency of pump

References

1. Mulder, M.M.; Hansen, A.C.; Mohammad, S.F.; Olsen, D.B. In Vitro Investigation of the St. Jude Medical Isoflow Centrifugal Pump: Flow Visualization and Hemolysis Studies. *Artif. Organs* **2008**, *21*, 947–953. [CrossRef] [PubMed]
2. Wheeler, F.G. The Adaption of the Centrifugal Pump to Chemical Problems. *J. Ind. Eng. Chem.* **1912**, *4*, 288–297. [CrossRef]
3. Dai, C.; Guo, C.; Chen, Y.; Dong, L.; Liu, H. Analysis of the Influence of Different Bionic Structures on the Noise Reduction Performance of the Centrifugal Pump. *Sensors* **2021**, *21*, 886. [CrossRef] [PubMed]
4. Duffy, D.C.; Gillis, H.L.; Lin, J.; Sheppard, N.F.; Kellogg, G.J. Microfabricated Centrifugal Microfluidic Systems: Characterization and Multiple Enzymatic Assays. *Anal. Chem.* **1999**, *71*, 4669–4678. [CrossRef]
5. Lim, A.E.; Lam, Y.C. Electroosmotic Flow Hysteresis for Fluids with Dissimilar PH and Ionic Species. *Micromachines* **2021**, *12*, 1031. [CrossRef]
6. Lim, A.; Goh, S. Effect of Microchannel Diameter on Electroosmotic Flow Hysteresis. *Energies* **2023**, *16*, 2154. [CrossRef]
7. Ni, D.; Yang, M.; Gao, B.; Zhang, N.; Li, Z. Numerical Study on the Effect of the Diffuser Blade Trailing Edge Profile on Flow Instability in a Nuclear Reactor Coolant Pump. *Nucl. Eng. Des.* **2017**, *322*, 92–103. [CrossRef]

8. Li, D.; Zhang, N.; Jiang, J.; Gao, B.; Alubokin, A.A.; Zhou, W.; Shi, J. Numerical Investigation on the Unsteady Vortical Structure and Pressure Pulsations of a Centrifugal Pump with the Vaned Diffuser. *Int. J. Heat Fluid Flow* **2022**, *98*, 109050. [CrossRef]
9. Ni, D.; Zhang, N.; Gao, B.; Li, Z.; Yang, M. Dynamic Measurements on Unsteady Pressure Pulsations and Flow Distributions in a Nuclear Reactor Coolant Pump. *Energy* **2020**, *198*, 117305. [CrossRef]
10. Ding, H.; Lin, F.; Chang, T.; Ge, F. Numerical Study on the Effect of Blade Trailing Edge Filing on Performance and Unsteady Pressure Pulsation in Low Specific Speed Centrifugal Pump. *J. Vib. Eng. Technol.* **2023**. [CrossRef]
11. Wei, J.; Xiangyuan, Z.; Hui, T.; Guojun, L.; Yuchuan, W. Numerical and Experimental Study of Influence of Semi-High Guide Vane on Pressure Fluctuation in Centrifugal Pump. *J. Cent. South Univ.* **2021**, *52*, 1276–1286.
12. Zhao, W.; Zhou, Z. Influence of Geometric Parameters of Tiny Blades on the Shroud of a Centrifugal Pump on the Cavitation Suppression Effect. *Front. Energy Res.* **2022**, *10*, 289. [CrossRef]
13. Gangipamula, R.; Ranjan, P.; Patil, R.S. Study on Fluid Dynamic Characteristics of a Low Specific Speed Centrifugal Pump with Emphasis on Trimming Operations. *Int. J. Heat Fluid Flow* **2022**, *95*, 108952. [CrossRef]
14. Wang, X.; Kuang, K.; Wu, Z.; Yang, J. Numerical Simulation of Axial Vortex in a Centrifugal Pump as Turbine with S-Blade Impeller. *Processes* **2020**, *8*, 1192. [CrossRef]
15. Cai, J.-C.; Chen, H.-J.; Brazhenko, V.; Gu, Y.-H. Study of the Hydrodynamic Unsteady Flow Inside a Centrifugal Fan and Its Downstream Pipe Using Detached Eddy Simulation. *Sustainability* **2021**, *13*, 5113. [CrossRef]
16. Posa, A.; Lippolis, A. Effect of Working Conditions and Diffuser Setting Angle on Pressure Fluctuations within a Centrifugal Pump. *Int. J. Heat Fluid Flow* **2019**, *75*, 44–60. [CrossRef]
17. Zhang, N.; Gao, B.; Ni, D.; Liu, X. Coherence Analysis to Detect Unsteady Rotating Stall Phenomenon Based on Pressure Pulsation Signals of a Centrifugal Pump. *Mech. Syst. Signal Process.* **2021**, *148*, 107161. [CrossRef]
18. Gülich, J.F. *Centrifugal Pumps*; Springer International Publishing: Cham, Switzerland, 2020; ISBN 978-3-030-14787-7.
19. Rodriguez, C.G.; Egusquiza, E.; Santos, I.F. Frequencies in the Vibration Induced by the Rotor Stator Interaction in a Centrifugal Pump Turbine. *J. Fluids Eng.* **2007**, *129*, 1428–1435. [CrossRef]
20. Spence, R.; Amaral-Teixeira, J. A CFD Parametric Study of Geometrical Variations on the Pressure Pulsations and Performance Characteristics of a Centrifugal Pump. *Comput. Fluids* **2009**, *38*, 1243–1257. [CrossRef]
21. Gao, B.; Guo, P.; Zhang, N.; Li, Z.; Yang, M. Unsteady Pressure Pulsation Measurements and Analysis of a Low Specific Speed Centrifugal Pump. *J. Fluids Eng.* **2017**, *139*, 071101. [CrossRef]
22. Yang, S.-S.; Liu, H.-L.; Kong, F.-Y.; Xia, B.; Tan, L.-W. Effects of the Radial Gap Between Impeller Tips and Volute Tongue Influencing the Performance and Pressure Pulsations of Pump as Turbine. *J. Fluids Eng.* **2014**, *136*, 054501. [CrossRef]
23. Kurniawan, K.E.; Santoso, B.; Tjahjana, D.D.D.P. Improvement of Centrifugal Pump Performance through Addition of Splitter Blades on Impeller Pump. In Proceedings of the 1st International Conference and Exhibition on Powder Technology Indonesia (ICePTi) 2017, Jatinangor, Indonesia, 8–9 August 2017; p. 030053.
24. Cavazzini, G.; Pavesi, G.; Santolin, A.; Ardizzon, G.; Lorenzi, R. Using Splitter Blades to Improve Suction Performance of Centrifugal Impeller Pumps. *Proc. Inst. Mech. Eng. Part J. Power Energy* **2015**, *229*, 309–323. [CrossRef]
25. Zhang, J.; Li, G.; Mao, J.; Yuan, S.; Qu, Y.; Jia, J. Effects of the Outlet Position of Splitter Blade on the Flow Characteristics in Low-Specific-Speed Centrifugal Pump. *Adv. Mech. Eng.* **2018**, *10*, 168781401878952. [CrossRef]
26. Li, G.; Zhang, J.; Mao, J.; Yuan, S.; Jia, J. Numerical Investigation of the Transient Flow and Frequency Characteristic in a Centrifugal Pump with Splitter Blades. *J. Therm. Sci.* **2021**, *30*, 562–573. [CrossRef]
27. Gu, Y.; Yuan, S.; Pei, J.; Zhang, J.; Zhang, F.; Huang, X. Effects of the Impeller–Volute Tongue Interaction on the Internal Flow in a Low-Specific-Speed Centrifugal Pump with Splitter Blades. *Proc. Inst. Mech. Eng. Part J. Power Energy* **2018**, *232*, 170–180. [CrossRef]
28. Wang, F.-J.; Qu, L.-X.; He, L.-Y.; Gao, J.-Y. Evaluation of Flow-Induced Dynamic Stress and Vibration of Volute Casing for a Large-Scale Double-Suction Centrifugal Pump. *Math. Probl. Eng.* **2013**, *2013*, 764812. [CrossRef]
29. Zhang, Z.C.; Wang, F.J.; Yao, Z.F.; Leng, H.F.; Zhou, P.J. Investigation on Impeller Radial Force for Double-Suction Centrifugal Pump with Staggered Blade Arrangement. *IOP Conf. Ser. Mater. Sci. Eng.* **2013**, *52*, 032009. [CrossRef]
30. Zeng, Y.; Yao, Z.; Wang, F.; Xiao, R.; He, C. Experimental Investigation on Pressure Fluctuation Reduction in a Double Suction Centrifugal Pump: Influence of Impeller Stagger and Blade Geometry. *J. Fluids Eng.* **2020**, *142*, 041202. [CrossRef]
31. Fu, D.-C.; Wang, F.-J.; Zhou, P.-J.; Xiao, R.-F.; Yao, Z.-F. Impact of Impeller Stagger Angles on Pressure Fluctuation for a Double-Suction Centrifugal Pump. *Chin. J. Mech. Eng.* **2018**, *31*, 10. [CrossRef]
32. Piomelli, U. Large-Eddy Simulation: Achievements and Challenges. *Prog. Aerosp. Sci.* **1999**, *35*, 335–362. [CrossRef]
33. Yang, Y.; Kær, S.K. Comparison of Reynolds Averaged Navier-Stokes Based Simulation and Large-Eddy Simulation for One Isothermal Swirling Flow. *J. Therm. Sci.* **2012**, *21*, 154–161. [CrossRef]
34. Braun, S. WINDOWS. In *Encyclopedia of Vibration*; Elsevier: Amsterdam, The Netherlands, 2001; pp. 1587–1595, ISBN 978-0-12-227085-7.
35. Ni, D.; Wang, F.; Gao, B.; Zhang, Y.; Huang, S. Experimental Investigation on the Effect of the Staggered Impeller on the Unsteady Pressure Pulsations Characteristic in a Pump. *Energies* **2022**, *15*, 8912. [CrossRef]